Influence of TBM geometry on lining loads of deep tunnels

V. De Gori
Geotechnical Design Group, Rome, Italy

A. de Lillis & S. Miliziano
Department of Structural and Geotechnical Engineering, Sapienza University of Rome, Rome, Italy

ABSTRACT: The paper presents a numerical study aimed at investigating the influence of the geometrical design of Tunnel Boring Machines (TBMs) on the forces acting on the lining. The study was conducted using a 3D numerical model that accounts for the major features of the excavation such as front pressure, overcut, shield conicity, tail void grouting, grout hardening over time and installation of the lining. To accurately reproduce the soil-shield-lining interaction, a simple procedure was adopted to overcome the modelling inaccuracies associated with the misidentification of the excavation profile due to the development of pre-convergences ahead of the excavation front. A parametric study was conducted to evaluate the influence of the shield's conicity and length on the lining forces. The results remark the great influence of the analysed parameters and show that the developed model can provide novel and significant insights on the interaction process.

1 INTRODUCTION

The structural design of tunnel linings must account for the stress release in the soil induced by the excavation and for the overall soil-shield-lining interaction process. This is particularly true for deep tunnels, in which the lining is subjected to high loads and high convergences are usually induced by design to reduce the stress state and minimize the shield's jamming risk.

Given the complexity of the soil behaviour and excavation process, empirical and analytical methods cannot provide solutions as accurate as those resulting from numerical modelling. 2D plane-strain numerical analyses though, suffer a series of shortcomings mainly related to the intrinsic three-dimensionality of the excavation process (Karakus, 2007). 3D modelling, on the other hand, allows to simulate realistically the main features of mechanized tunnelling and can yield satisfactory results (Kasper & Meschke, 2004; Litsas et al., 2018; Losacco & Viggiani, 2019; Miliziano & de Lillis, 2019).

Although recent improvements in computational power have made 3D modelling significantly more affordable, the time and skills required to develop and fine-tune the models and the actual runtime can still bottleneck the design process. Among the main factors to be accounted for, the following require special consideration: i) the face pressure applied by the front of the TBM (and by the muck inside the excavation chamber in case of Earth Pressure Balance TBMs); ii) the geometry of the TBM, including the overcut and the conicity of the shield, which are still often overlooked; iii) the annular void behind the tail of the machine; iv) the grouting of the tail void, its mechanical properties and their evolution over time. The structural system of the segmental lining has been studied by several authors with somewhat mixed results (e.g. Arnau & Molins, 2012; Do et al., 2014). Kavvadas et al. (2017) proposed a comparison of lining forces obtained simulating the lining in three different ways (i.e. continuous shell, shells with aligned joints and shells with staggered joints) and found the resulting differences to be quite small.

This study focuses on the influence of the geometrical design of the TBM on the soil-shield-lining interaction process and, ultimately, on the lining forces. Specifically, an advanced 3D numerical model was developed accounting for the main factors influencing the problem and used to investigate the influence of the shield's conicity and length. The model is founded on a very accurate geometric and mechanical representation and the excavation is simulated in detail. The model, which was tested satisfactorily against monitoring data by De Gori et al. (2019), is fine-tuned for deep tunnelling in soft ground. Also, the model adopts a simple numerical procedure, proposed by de Lillis et al. (2018), to overcome modelling issues associated with the misidentification of the actual excavation boundary induced by the development of pre-convergences (radial soil displacements ahead of the excavation front).

The analyses are performed in effective stresses and, assuming clayey soils, the tunnel excavation is

simulated in undrained conditions. Once a stationary solution is reached, drained conditions are simulated. The effects of gravity (and also the weight of the shield and the lining) are neglected.

In the following, after a brief description of the numerical model and the mesh design technique, the main results are illustrated and discussed, focussing on the decisive influence of the soil-shield interaction on the forces arising in the lining.

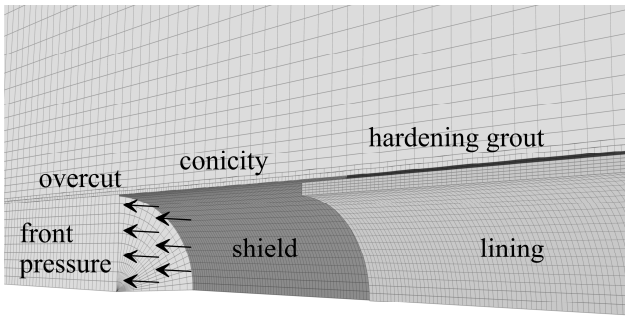

Figure 1. Main features of the simulation scheme.

2 NUMERICAL MODEL

The numerical model, developed with the finite difference code FLAC3D, simulates the main factors affecting the soil-shield-lining interaction, namely: front pressure at the excavation face, overcut, conicity (tapering) of the shield, annular tail void behind the shield, void grouting and grout hardening over time, installation of the lining and application of the jacks thrust (Fig. 1). The model is fine-tuned for deep mechanized tunnels; as such, the effects of gravity can be neglected and, taking advantage of the resulting plane of symmetry, just one quarter of the problem can be modelled.

The mesh size and density (Fig. 2) were thoroughly checked to ensure negligible boundary effects and a proper accuracy of the simulation of the TBM's geometry and the interaction process, especially close to the tunnel. Furthermore, the model works in large-strain mode, thus, the position of the grid nodes is updated at the end of each calculation step. This enhances the simulation of the contacts between moving grids due to lower geometrical tolerances.

TBMs for deep tunnels are usually designed to minimise the risk of jamming and the lining forces. For this reason, the overcut and the conicity are wilfully increased to magnify the steering gap and the stress relaxation. Clearly, in such cases, higher care must be placed in the accurate identification of the excavation boundary.

The shield of the TBM is simulated via very stiff elastic continuum elements, whose geometrical properties are reported in Table 1 together with those of the lining. The lining is also simulated using elastic continuum elements (Augarde & Burd, 2001), with a Young's modulus of 37.2 GPa, neglecting the presence of joints. Both the lining and the shield are assumed to be weightless. On the external surface of the shield, an elastic interface is applied. The stiffness of the interface was calibrated checking the system's behaviour during contacts and ensuring the absence of overlapping between soil and shield grid points. The forces exerted by the hydraulic jacks on the lining are simulated as a uniform longitudinal pressure.

The soil mechanical behaviour is described adopting the CYsoil model; an elastic-plastic constitutive model with hardening, both deviatoric and volumetric, characterized by an elliptic volumetric cap and a frictional Mohr-Coulomb shear envelope (Itasca, 2012). It is a model able to describe with sufficient accuracy the non-linearity of the soil behaviour. The main soil parameters are listed in Table 2 where, with reference to effective stresses, φ is the friction angle, c the cohesion, υ the Poisson's ratio, ψ the dilatancy angle, E^0_{ref} the reference Young's modulus, p_{ref} the reference mean pressure, R_f the failure ratio and β a calibration factor. The initial stress state is: total vertical stress σ_v = 1800 kPa, total horizontal stress σ_h = 1300 kPa, pore pressure u = 500 kPa. The soil is normally consolidated and the at-rest coefficient of lateral earth pressure K_0 is 0.615, adopting Jaky's law. At this stage of the study, the soil is assumed to be able to withstand any value of suction.

The excavation is simulated adopting a step-by-step approach, which involves the following substeps: 1) the excavation advances one ring (1.2 m) and the corresponding soil slice is removed; 2) the shield moves forward and applies the front pressure to the new excavation face; 3) the lining ring installed in the previous phase is now outside the shield; a new ring is generated and the jacks thrust is applied; 4) the algorithm reads the current position of the soil and the tail void is injected with grout; previously injected grout is hardened following the law proposed by Kasper & Meschke (2006) and assuming an advancement rate of the excavation of 12 m/day.

The analyses are carried out in effective stresses and the excavation is simulated in undrained conditions, imposing total volumetric deformations equal to zero everywhere in the domain, assuming a low-permeability fine-grained soil and thus a negligible dissipation of excess pore pressure in the surrounding

Table 1. TBM and lining geometry.

Cutterhead radius (m)	Shield front radius (m)	tail radius (m)	length (m)	Lining extrados radius (m)
2.5	2.48	2.43	8	2.38

Table 2. Main soil parameters.

φ (°)	c (kPa)	υ (-)	ψ (°)	E^0_{ref} (MPa)	p_{ref} (kPa)	R_f (-)	β (-)
22	0	0.3	0	15	100	0.85	5

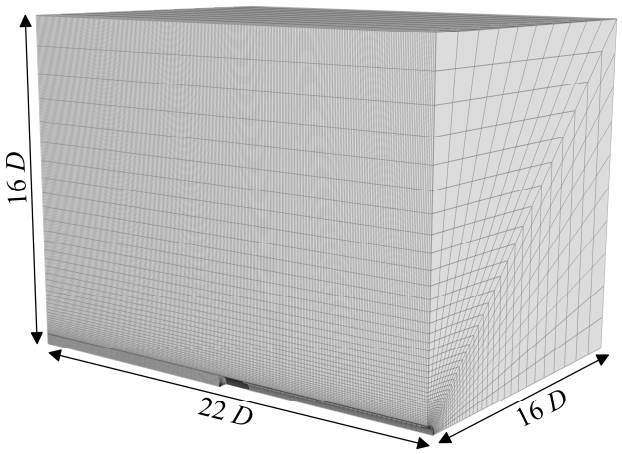

Figure 2. Numerical model.

soil. Upon reaching a stationary solution (about 4 diameters, *D*, behind the tail), long-term drained conditions are simulated re-imposing the initial pore pressure in the entire calculation domain.

2.1 *Mesh design*

Most numerical models adopt a mesh initially designed to have grid nodes located on the excavation boundary. This allows to instruct the excavation algorithm to remove the slice of soil inside those nodes once the TBM passes through a generic section. Since the stress release induced by the excavation propagates beyond the tunnel face, though, pre-convergences (radial displacements ahead of the excavation front) develop and the above-mentioned grid nodes move inside the excavation boundary (Fig. 3a). This means that the algorithm will "excavate" a portion of soil which is smaller than the actual excavation, dictated by the diameter of the cutting wheel. Furthermore, this entails that the subsequent interaction process will start from a configuration in which the soil nodes are at the wrong distance from the shield. Also, if the starting stress state is anisotropic, the soil nodes will not be equidistant from the tunnel axis due to the pre-convergences being anisotropic as well.

To tackle this issue, a simple technique proposed by de Lillis et al. (2018) was adopted. The procedure consists in designing a starting mesh that correctly reproduces the actual excavation profile after the development of the pre-convergences. To this aim, a trial analysis is performed adopting a standard circular mesh and recording the pre-convergences along the tunnel wall. Then, the recorded values are added radially to the starting location of the nodes obtaining an elliptical mesh (being the pre-convergences asymmetrical given the anisotropic starting stress state) that will coincide with the excavation diameter after the pre-convergences (Fig. 3b). Even though it is an iterative procedure, one iteration usually provides satisfactory results.

3 NUMERICAL RESULTS

In this paragraph, some of the main results are described, focusing on the development of radial displacements (convergences) in the soil, the soil-shield-lining interaction and the resulting lining forces induced by the passage of TBM in undrained conditions, at first, and then in long-term conditions.

Figure 4 shows the longitudinal profile of the radial position of two soil points located at the crown and at the springline. The oscillations in the results are due to the excavation advancing step-by-step 1.2 m at a time. When the excavation moves forward the soil nodes in the newly excavated stretch are at different distances from the excavation front and thus respond differently. The starting position of the nodes is different because the pre-convergences, given the initial asymmetrical stress state, will be asymmetrical (smaller at the springline and higher at the crown). As anticipated, the mesh is designed in such a way that, when a given section is to be excavated, the location of the soil nodes coincides with that of the actual ex-

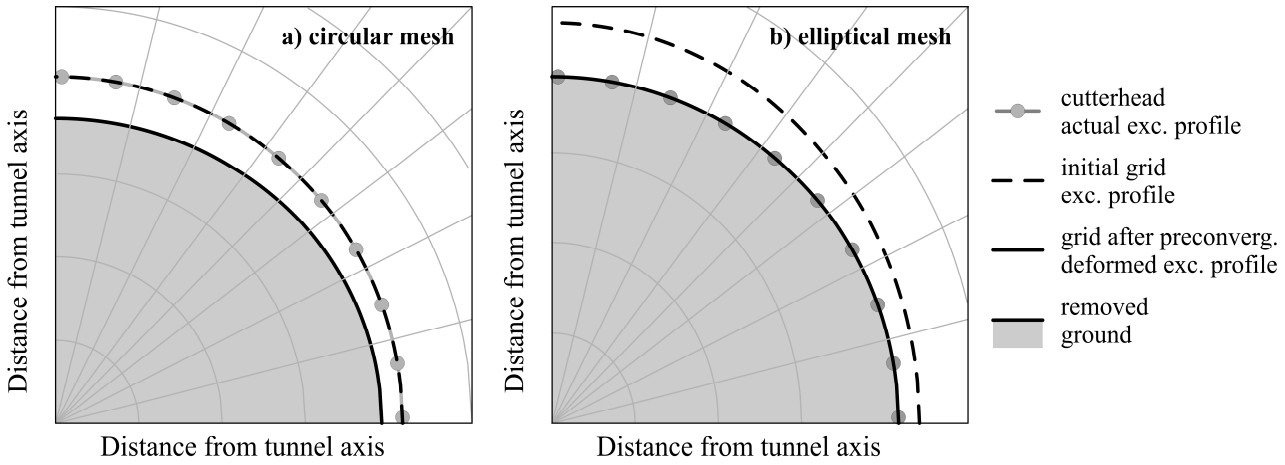

Figure 3. Mesh design: a) circular mesh; b) elliptical mesh.

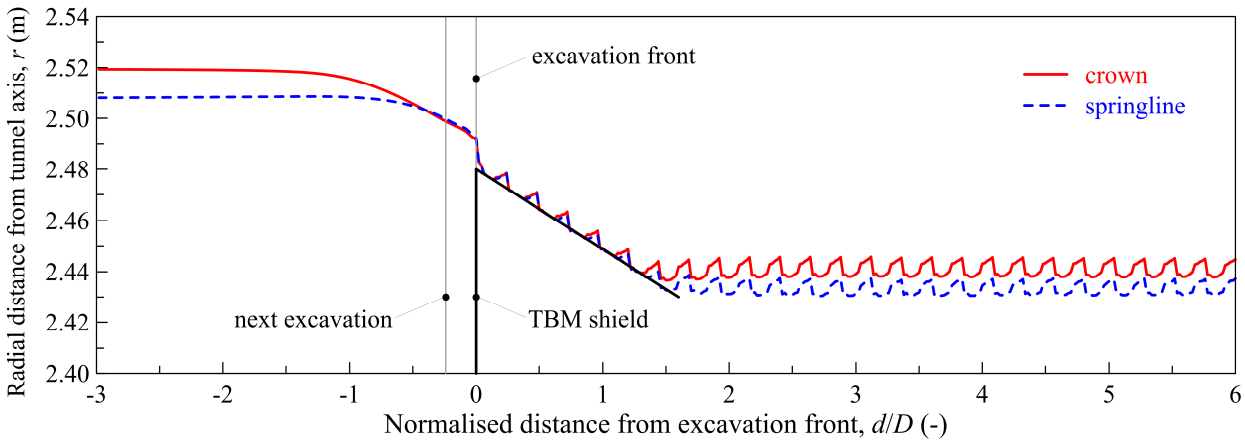

Figure 4. Longitudinal profile of radial displacements.

cavation boundary. After the excavation, more displacements develop and the soil tends to close on the machine's shield, following its conicity. At the tail of the machine, the radial distance from the tunnel axis is smaller at the springline due to a more plastic behaviour. Roughly 4 diameters behind the excavation face, three-dimensional effects fade and stationary undrained conditioned are attained after the injection of the grout and its hardening.

The described behaviour can be further illustrated by looking at the longitudinal profile of the radial stresses in the soil (Fig. 5). About 1.5 diameters ahead of the excavation front, a slight rise in radial stresses, due to the development of a 3D arch, can be observed. Then, the stresses decrease rapidly and become zero at the excavation face, where the overcut generates a void (there is no contact between soil and shield).

Behind the front face, because of the high initial stress state and its poor mechanical properties, the soil closes abruptly onto the shield and the radial stresses increase again once contact is established. Due to the stress release induced by the excavation, the radial stress decreases and the circumferential stress increases around the tunnel, causing a stronger increase of the deviatoric stress near the springline. This redistribution of stresses is associated with a more plastic behaviour near the side of the tunnel, as shown in Figure 6, where the mobilised friction angle at different distances from the excavation face is reported.

As the excavation face gets further (Fig. 5), the conicity of the shield allows further displacements in the soil and the radial stresses progressively decrease. Near the tail, the stress is zero at the crown, where there is no contact with the shield. Behind the TBM, the annular tail void is injected with grout and the radial stresses increase.

Overall, the changes in the stress field induced by the excavation and the soil-shield interaction are such that at the tail of the machine the stress state is the opposite of the starting one, with the radial stress being higher at the springline. The forces induced in the lining are generated by the interaction with this, new, profoundly changed, stress distribution in the soil.

The normal force N and the bending moment M in stationary undrained conditions and in drained conditions are shown in Figure 7. The axial forces range between 1850 kN and 2000 kN in undrained condition (Fig. 7a); the minimum value being at the springline and the maximum at the crown. The bending moment, quite small in absolute values, is negative (internal fibers elongated) at the springline and positive at the crown (Fig. 7b). The maximum compres-

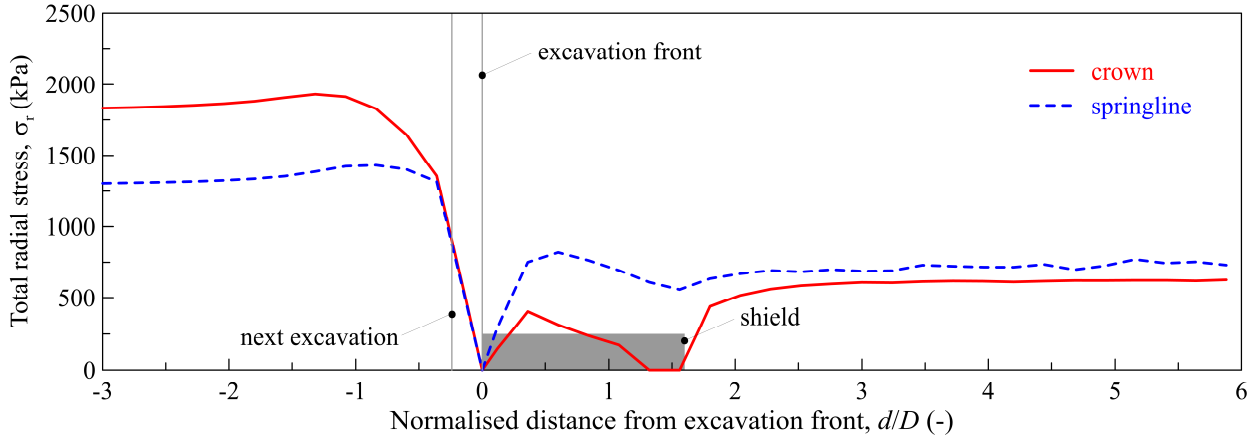

Figure 5. Longitudinal profile of radial stresses.

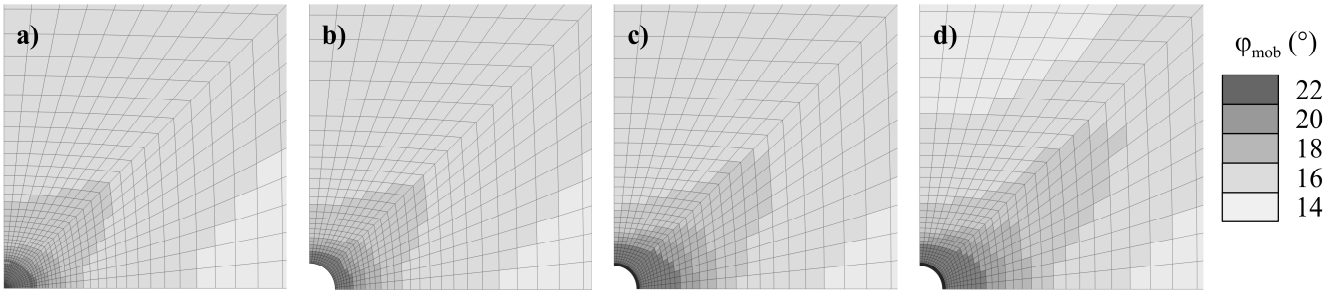

Figure 6. Evolution of the mobilised friction angle: a) 1*D* ahead of the excavation front; b) at the excavation front; c) after the grout injection; d) undrained stationary conditions.

sive stress in the lining (σ_c), calculated assuming a homogeneous concrete section, is higher at the crown and lower at an angle of about 45° along the tunnel wall (Fig. 7c).

The internal forces can be related with the longitudinal profile of the radial stresses seen in Figure 5. In fact, the higher normal force at the crown is associated with the higher radial stress near the springline, and vice versa. The small difference between the radial stresses induces small variability of the axial forces along the tunnel wall and small values of bending moments.

In long-term drained conditions, the dissipation of the negative excess pore pressure induced by the excavation induces an appreciable increase of the normal forces, which reach values between 2100 kN and 2250 kN; the bending moment changes are very small; the maximum compressive stress rises almost uniformly due to the increase of *N*.

A set of parametric analyses was carried out to investigate the influence of changes in the TBM geometry on the forces induced in the lining. In particular, the study focused on the influence of the conicity and length of the shield.

3.1 *Influence of the shield's conicity*

At first, two analyses were performed increasing the shield's conicity, *c*, from 5 cm to 7.5 cm ($c_{7.5}$-analysis) and 10 cm (c_{10}-analysis); all the other inputs of the analyses were kept the same.

As seen in the previous paragraph, the lining forces are closely related to the radial displacement and the evolution of stresses, especially radial ones, in the surrounding soil. The results of the analyses, reported in Figure 8 in terms of radial position of the soil nodes located at the crown and at the springline, show that, as the conicity of the shield increases, the pre-convergences increase (appreciably going from c_5 to $c_{7.5}$, much less from $c_{7.5}$ to c_{10}) and the soil closure onto the shield decreases. The increase in conicity forces the soil to displace more to reach a contact point. Near the tail of the shield, the contact does not materialize along a portion of the shield that grows larger as the conicity increases, thanks to 3D effects allowing a stable configuration even though the soil-shield contact is incomplete. In particular, this is possible because of the contact points located near the excavation face and behind the tail of the machine, where grout has been injected.

At the rear end of the shield, the soil is in contact with the shield at the side of the tunnel wall, in the springline area, with the notable exception of the c_{10}-analysis.

From a stress point of view, this means that near the tail of the TBM, the radial stresses are zero at the crown for a longitudinal stretch that increases with *c*, while they are greater than zero in the springline area. In the c_{10}-analysis, instead, since there is a residual void near the springline too, the radial stresses are zero all along the tunnel wall.

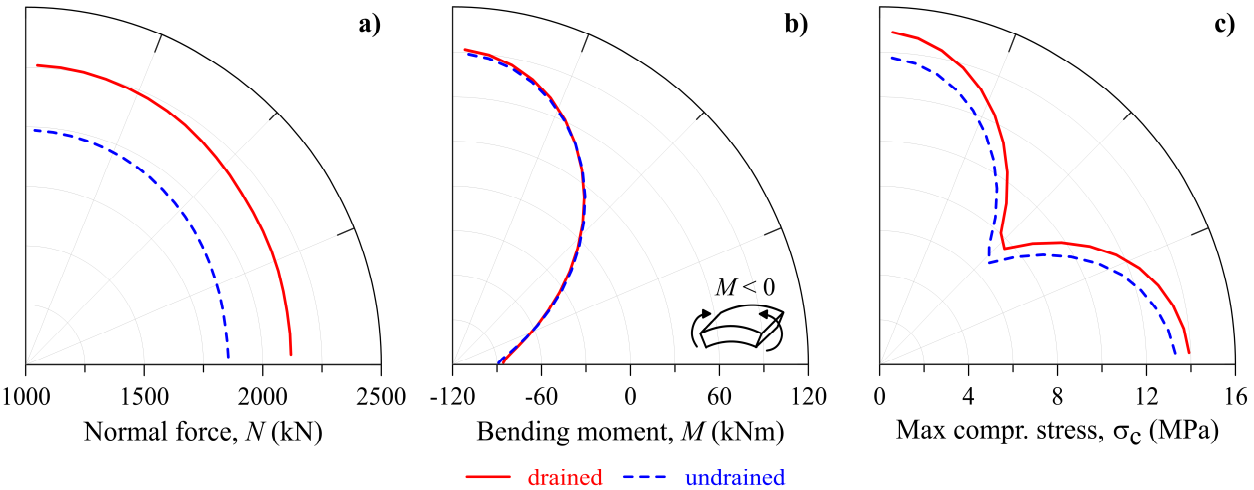

Figure 7. Stress state in the lining: a) normal force; b) bending moment; c) maximum compressive stress.

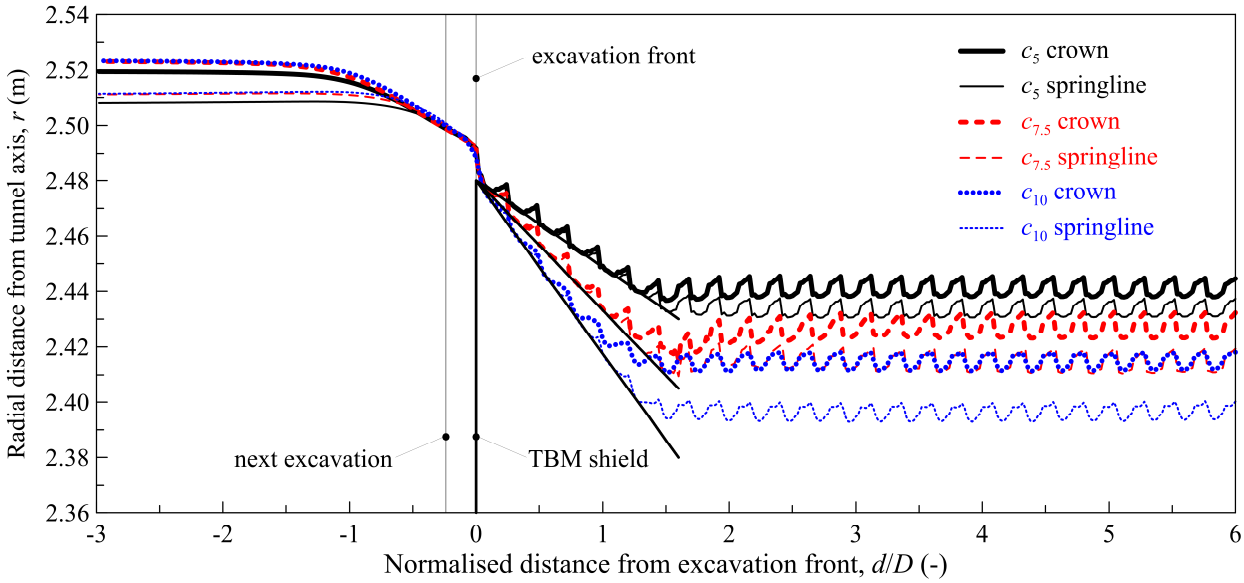

Figure 8. Influence of the shield's conicity on the radial displacements.

As discussed in the previous paragraph, the stress-displacement field at the tail of the machine, has a decisive influence on the lining forces.

The greater the shield's conicity, the greater the stress relaxation in the surrounding soils. Thus, as the conicity increases, the normal force in the lining decreases (Fig. 9a). The distribution of N resulting from the c_{10}-analysis, differs qualitatively from the others: in this case the soil does not touch the shield's tail at any point (the radial stresses are zero both at the crown and at the springline), and this leads to a different interaction process. As c increases, the variability of N along the tunnel wall decreases, inducing smaller bending moments (Fig. 9b). These distributions result in the maximum compressive stress decreasing as c increases. Particularly, σ_c is 20% and 40% smaller than the reference case, respectively in the $c_{7.5}$ and the c_{10} analyses (Fig. 9c).

It is worth to point out that greater displacements are obviously associated with a more plastic behaviour and an increase of the plastic radius around the tunnel, which could, in some cases, induce local failures in the surrounding soil.

In drained conditions, the normal forces increase uniformly while the bending moments do not vary significantly. In particular, a greater increase in N is observed in the analyses with larger conicities. This is clearly related to the amount of negative excess pore pressure developed during the excavation, which grow larger with the conicity and the associated stress relaxation.

3.2 *Influence of the shield's length*

Two further analyses were performed investigating the influence of the shield's length on the longitudinal displacements and the lining forces. The shield's

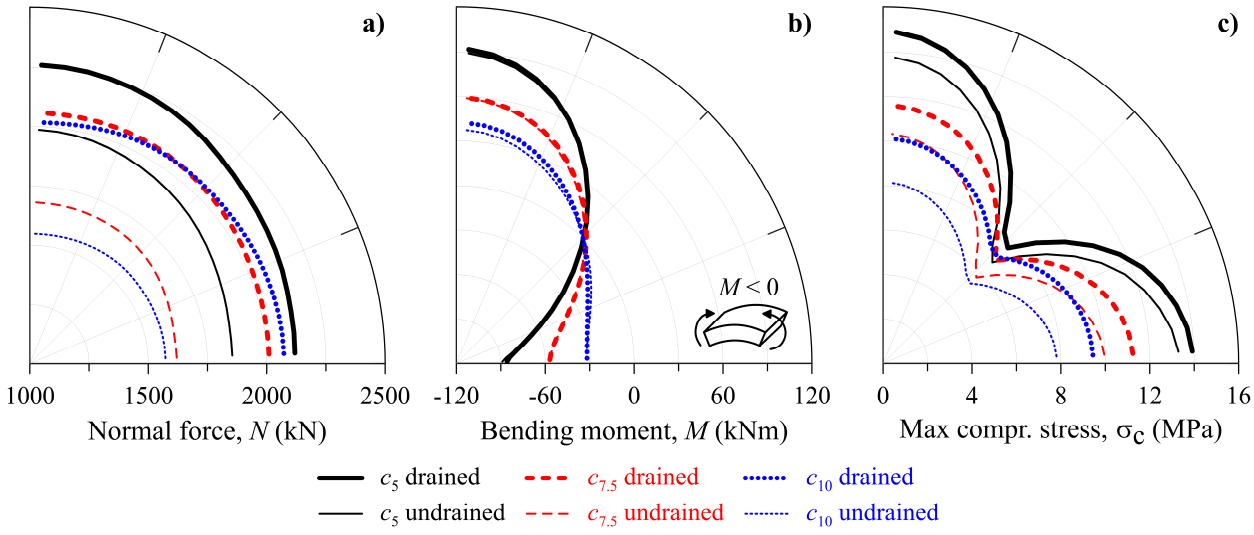

Figure 9. Influence of the shield's conicity on the lining loads: a) normal force; b) bending moment; c) maximum compressive stress.

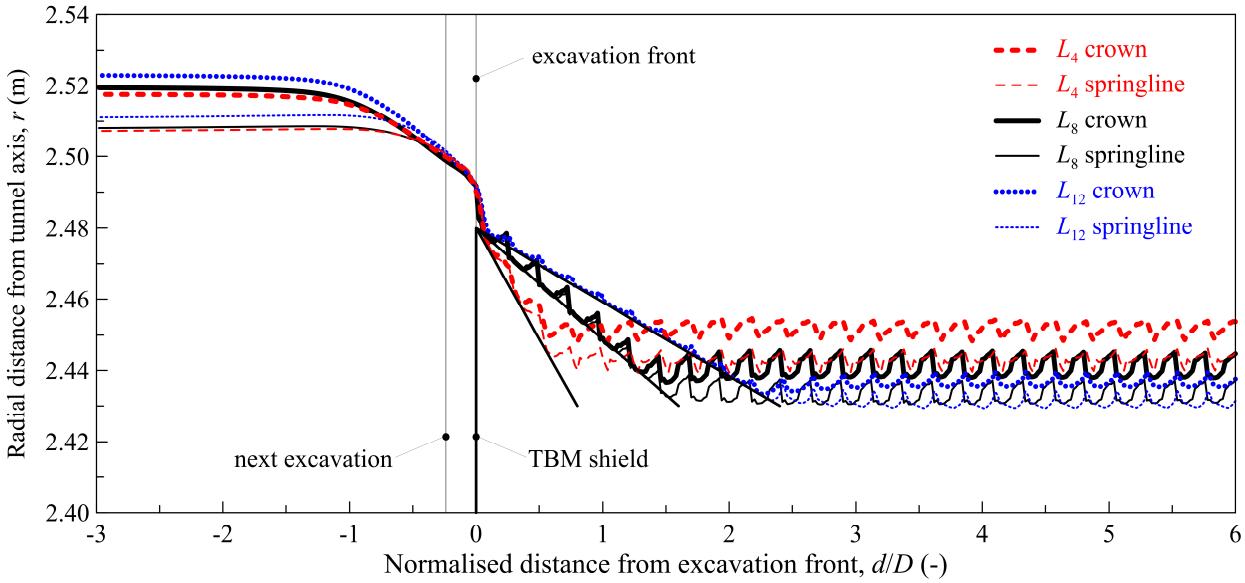

Figure 10. Influence of the shield's length on the radial displacements.

length, L, was assumed to be 4 m (L_4-analysis) and 12 m (L_{12}-analysis) respectively, while keeping constant all the other inputs.

Figure 10 shows the longitudinal displacements profiles. The results show that as L increases, both the pre-convergences and the portion of the shield along which the soil touches the TBM increases. Assuming a 4m-long shield, the soil does not close onto the shield because a stable configuration can be achieved thanks to the short distance between the excavation face and the injected annular void (strong 3D effects). Assuming a 12m-long shield, instead, the soil displaces more gradually, as the stabilizing 3D effects induced by the closeness of the excavation front fade moving further along the shield.

In terms of lining forces (Fig. 11), the results show that the stress relaxation is directly related to the shield's length; thus, N decreases as L increases. Conversely, the variability of N along the tunnel wall, and thus M, increases appreciably with the length of the shield.

The similarity between the results obtained from the L_8 and the L_{12} analyses can be explained looking at the longitudinal displacement profile: in both cases the shield is long enough to ensure weak 3D effects, resulting in similar behaviours. In both analyses, in fact, the soil touches the shield along the majority of its length and only at its tail, in the crown area, a gap persists.

As seen in the c_{10}-analysis, the distribution of N resulting from the L_4-analysis is different from the others. Once again, this is due to the radial stresses being zero all along the tunnel wall at the tail of the shield (while in the other cases $\sigma_r = 0$ just near the crown), leading to a strongly different soil-lining interaction.

In drained conditions, the normal forces increase homogeneously in all the analyses, while the bending

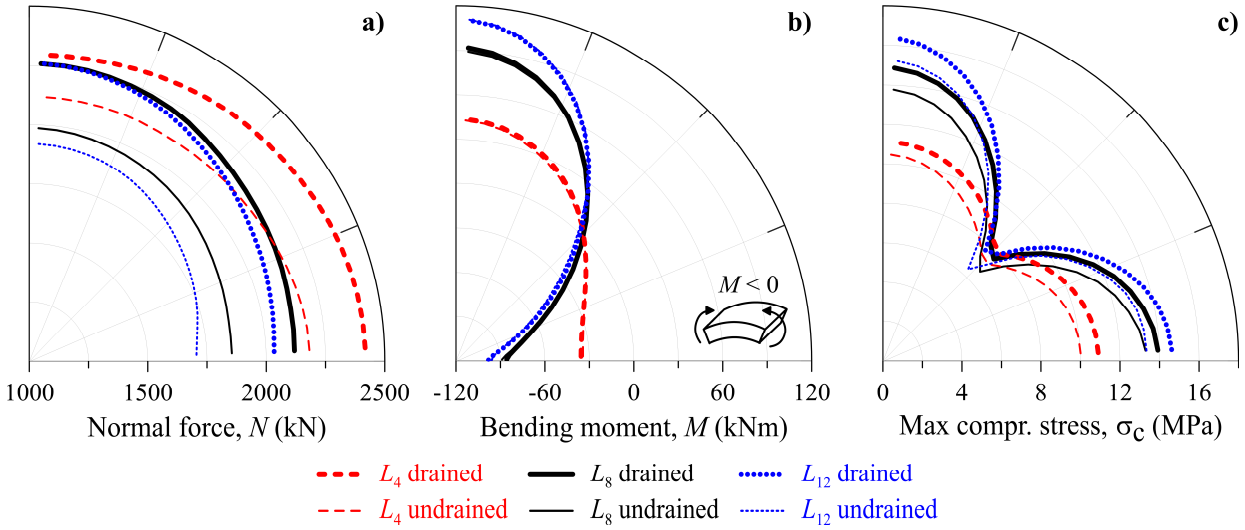

Figure 11. Influence of the shield's length on the lining loads: a) normal force; b) bending moment; c) maximum compressive stress.

moments does not vary significantly. In particular, the increase in N due to the consolidation process increases slightly with L. In terms of maximum compressive stress, the case of L = 4 m, provides maximum values which are about 30% lower than the case with the longer shield.

4 CONCLUSIONS

To accurately predict the lining loads of deep tunnels, the stress release induced in the soil by the excavation must be accounted for. This paper presented an advanced 3D numerical model that simulates the main features of mechanized tunnelling with remarkable geometrical accuracy. Moreover, a numerical procedure to avoid the misidentification of the excavation boundary is adopted.

Under the assumptions made in this study (gravity is neglected, as is the weight of the shield and the lining, undrained soil-shield-lining interaction during the excavation, final drained condition achieved without studying the consolidation process), the numerical results show that the soil-shield-lining interaction causes a great stress redistribution around the tunnel, primarily associated with 3D effects and soil-shield contacts. The resulting lining loads depend on the soil stress state at the rear end of the shield, which in most cases was found to be the opposite of the initial K_0 stress state (horizontal stress at the springline higher than the vertical stress at the crown). This phenomenon is due to a complex interaction with the shield of the TBM, characterized by a localized contact at the springline and a residual gap near the crown.

The parametric analyses show that the geometry of the TBM has a great influence on the stress state of the lining. As the conicity increases the stress relaxation increases and the resulting stress state in the lining is smaller and more homogeneous. In the investigated cases, the maximum compressive stress decreases by 25% and 40% as the conicity increases by 50% and 100%, respectively. Of course, as the conicity increases, larger plastic zones will develop and the extension of the areas where the shear strength is fully mobilized will increase.

The length of the shield has a significant influence on the development of 3D effects; if the machine is short enough, a strong longitudinal arch can develop between the soil in contact with the injected grout (behind the tail) and the soil just ahead of the excavation front, profoundly altering the entire interaction. Such phenomena can only be observed performing advanced 3D analyses, as the ones presented herein.

The results provide novel insights on the soil-shield-lining interaction process and further developments shall have significant implications on both the geometrical design of TBMs and the structural design of deep tunnel linings.

REFERENCES

Arnau, O. & Molins, C. 2012. Three dimensional structural response of segmental tunnel lining. *Engineering Structures* 44: 210-221.

Augarde, C.E. & Burd, H.J. 2001. Three-dimensional finite element analysis of lined tunnels. *International Journal of Numerical and Analytical Methods in Geomechanics* 25(3):243–262.

De Gori, V., de Lillis, A. & Miliziano, S. 2019. Lining stresses in a TBM-driven tunnel: a comparison between numerical results and monitoring data. In D. Peila, G. Viggiani & T. Celestino (eds.), *Tunnels and Underground Cities: Engineering and Innovation meet Archaeology, Architecture and Art; Proceedings of the WTC 2019 ITA-AITES World Tunnel Congress, Naples, 2019.* London: CRC Press.

de Lillis, A., De Gori, V. & Miliziano, S. 2018. Numerical modelling strategy to accurately assess lining stresses in mechanized tunnelling. In A.S. Cardoso, J.L. Borges, P.A. Costa, A.T. Gomes, J.C. Marques & C.S. Vieira (eds.), Proceedings of the *9th European Conference on Numerical Methods in Geotechnical Engineering, Porto, 2018*. London: CRC Press.

Do, N.A., Dias, D., Oreste, P. & Djeran-Maigre, I. 2014. Three-dimensional numerical simulation for mechanized tunnelling in soft ground: the influence of the joint pattern. *Acta Geotechnica* 9(4): 673-694.

Itasca Consulting Group, Inc. 2012. FLAC3D Version 5.0, Fast Lagrangian Analyses of Continua in Three-Dimensions, User's manual. Minneapolis.

Karakus, M. 2007. Appraising the methods accounting for 3D tunnelling effects in 2D plane strain FE analysis. *Tunnelling and Underground Space Technology* 22(1): 47–56.

Kasper, T. & Meschke, G. 2004. A 3D finite element simulation model for TBM tunnelling in soft ground. *International Journal for Numerical and Analytical Methods in Geomechanics* 28(14): 1441–1460.

Kasper, T. & Meschke, G. 2006. On the influence of face pressure, grouting pressure and TBM design in soft ground tunnelling. *Tunnelling and Underground Space Technology* 21(2): 161–171.

Kavvadas, M., Litsas, D., Vazaios, I. & Fortsakis, P. 2017. Development of a 3D finite element model for shield EPD tunnelling. *Tunnelling and Underground Space Technology* 65: 22–34.

Litsas, D., Sitarenios, P. & Kavvadas, M. 2018. Parametric investigation of tunnelling-induced ground movement due to geometrical and operational TBM complexities. *Italian Geotechnical Journal* 51(4): 22–34.

Losacco, N. & Viggiani, G.M.B. 2019. Class A prediction of mechanised tunnelling in Rome. *Tunnelling and Underground Space Technology* 87:160–173.

Miliziano, S. & de Lillis, A. 2019. Predicted and observed settlements induced by the mechanized tunnel excavation of metro line C near S. Giovanni station in Rome. *Tunnelling and Underground Space Technology* 86: 236-246.